How to cite: *Angew. Chem. Int. Ed.* **2025**, e202512482
doi.org/10.1002/anie.202512482

Heterogeneous Catalysis **Very Important Paper**

Harnessing the Dynamic Nature of a Zirconium-Oxo Nanocluster for Reversible Protein Capture and Proteolysis

Kilian Declerck, Nada D. Savić, Muhammed Jibin Parammal, Carlotta Seno, Gilles Bruylants, Jonathan De Roo, and Tatjana N. Parac-Vogt**

Abstract: Selective proteolysis remains a significant challenge with relevance to industrial and pharmaceutical applications, motivating development of chemical strategies emulating the specificity of natural proteases. Here, we report that the discrete Zr-oxo nanocluster-based solid, $[Zr_{17}O_8(OH)_{24}(OH_2)_{12}(HCO_2)_{12}(SO_4)_8] \cdot 6\ HCl \cdot 30\ H_2O$ (Zr_{17}) serves as an efficient, recyclable heterogeneous catalyst for site-selective proteolysis with tunable fragment selectivity. A combination of solution- and solid-state NMR spectroscopy highlighted the importance of the ligand environment of solid Zr_{17} for enabling efficient protein-cluster interaction and controlling reactivity. We demonstrate that Zr_{17} achieves a proteolytic performance comparable to natural enzymes while allowing fine modulation of peptide product profiles by adjusting reaction parameters. Substrate adsorption and product desorption were found to be governed by the net charge of both catalyst and substrate, as well as rapid reorganization of the cluster's capping ligands, according to UV-Vis/IR spectroscopy and isothermal titration calorimetry. Crucially, the insoluble nature and excellent stability of Zr_{17}, evidenced by pair distribution function analysis, allowed reuse across multiple catalytic cycles, overcoming a major limitation of proteolytic systems. This study reveals how cluster surface chemistry governs substrate interaction and catalysis, guiding rational design of next-generation cluster-based catalysts, including hybrid materials such as metal-organic frameworks.

Introduction

Protein hydrolysis is an essential process in a biological context, by playing a key role in cellular regulation, and in an industrial context, where it contributes to numerous operations ranging from textile processing to waste decomposition.[1–3] It also facilitates biotechnological applications, ranging from protein characterization in the field of proteomics to treatment of protein-related diseases such as Huntington's and Alzheimer's disease.[4–9] Enzymatic protein degradation, the most widely used approach, offers high specificity but is inherently constrained by factors such as narrow substrate scope, sensitivity to fluctuations in pH and temperature, and susceptibility to an array of inhibiting factors.[10,11] These limitations restrict their applicability in systems where precise and controlled cleavage of proteins under diverse conditions is required, such as in the characterization of heterogeneous protein samples or in industrial applications that demand extreme conditions for increased efficiency, for example, waste management or food processing.[12–14] Furthermore, proteases often require specific reaction conditions that may not be compatible with requirements of large-scale applications, necessitating costly optimization and stabilization strategies.[11,15–18]

Considering these challenges, there is increasing interest in developing alternative catalysts that can achieve selective and controlled proteolysis without the drawbacks associated with the enzymatic methods. A key objective in this pursuit is identification of factors that govern cleavage efficiency and selectivity, allowing for tunable reactivity across various substrates and conditions.[19] The structural properties of catalytic systems and the reaction conditions are crucial factors that influence hydrolysis efficiency and selectivity. A more thorough understanding of these parameters could enable more rational design of catalysts that not only match the efficiency of natural proteases but surpass them in versatility, paving the way for broader implementation. To this extent, our group has been developing a diverse series of metal-based catalysts, ranging from soluble metal-oxo clusters (MOCs), such as Zr-substituted polyoxometalates (Zr-POMs) and $[Zr_6O_4(OH)_4(CH_3CO_2)_8(H_2O)_2Cl_3]^+$ (Zr_6), to insoluble metal-organic frameworks (MOFs) that are able to reliably cleave proteins into large polypeptides under diverse reaction conditions.[19–24] The high Lewis acidity of Zr(IV) centers facilitates coordination and activation of the peptide bond, enabling nucleophilic attack of water and hydrolysis.[21,25] Previous studies have shown that

[*] K. Declerck, Dr. N. D. Savić, Prof. Dr. T. N. Parac-Vogt
Department of Chemistry, KU Leuven, Celestijnenlaan 200F, Leuven 3001, Belgium
E-mail: nada.savic@kuleuven.be
tatjana.vogt@kuleuven.be

M. J. Parammal, C. Seno, Prof. Dr. J. De Roo
Department of Chemistry, University of Basel, Mattenstrasse 22, Basel 4058, Switzerland

Prof. Dr. G. Bruylants
Faculty of Applied Sciences, Université Libre de Bruxelles, Avenue FD Roosevelt 50, Brussels 1050, Belgium

Additional supporting information can be found online in the Supporting Information section

the efficiency and selectivity of peptide bond hydrolysis are governed by the Zr(IV) center and its coordination environment, ensuring controlled proteolysis and facilitating analysis of the resulting mass spectrometry data.[20,26] Interestingly, most Zr(IV) cluster-based catalysts specifically cleave the peptide bond next to aspartate residues, generating peptide fragments in the size range between 3 and 15 kDa, which are ideal for middle-down proteomics. Many proteases, such as the frequently used trypsin, create shorter fragments and most chemical agents lack sufficient specificity to reliably produce larger polypeptides.[18,20,22,27]

MOFs, as insoluble materials, catalyze proteolysis heterogeneously, as opposed to soluble metal-oxo clusters such as Zr-POMs and Zr_6. However, protein-MOF interactions remain largely unexplored due to significant protein adsorption on the MOF's intricate surface. In addition, while insoluble catalysts allow for straightforward separation from the protein digest, facilitating catalyst recycling, MOFs have mainly demonstrated reusability for hydrolysis of simple dipeptides.[24,28–30] This limitation stems from excessive protein adsorption and accumulation of peptide fragments on the MOF surface, which is challenging to reverse. In addition to extended metal-based materials like MOFs, a recent study has established the potential of an insoluble Hf-based cluster, $Hf_{18}O_{10}(OH)_{26}(SO_4)_{13}(H_2O)_{33}$ (Hf_{18}), which exhibited aspartate selective cleavage of myoglobin.[27] Due to the discrete nature of the Hf_{18} cluster, protein adsorption at its surface was anticipated to be more controllable in comparison to the porous structure of MOFs, where diffusion limitations and interference from hydrophobic interactions originating from the organic linkers cause more complex adsorption behavior.[27,31–33] However, despite the promising reactivity of Hf_{18}, the elution process required for desorption of peptide fragments resulted in catalyst deactivation, also preventing in-depth investigation of the protein-cluster interactions at the molecular level.[27]

Achieving reversible adsorption/desorption of protein and fragments from materials is a challenging task, but we anticipated that it can be achieved by carefully selecting both the ligands surrounding the cluster and the reaction medium. The capping ligands coordinated to the cluster are key to governing the stability of both the cluster and substrate-cluster intermediates formed in solution. Therefore, understanding and controlling the ligand exchange process in solution is essential to regulate substrate coordination and adsorption/desorption while also providing valuable insights into the reaction mechanism. In order to accomplish this, we focused on the development of a metal-oxo cluster capped with diverse ligands that can be exchanged without compromising the cluster's stability and reactivity. Specifically, solid 17-nuclear Zr-oxo cluster stabilized by formate and sulfate ligands, $[Zr_{17}O_8(OH)_{24}(OH_2)_{12}(HCO_2)_{12}(SO_4)_8] \cdot 6\,HCl \cdot 30\,H_2O$ (Zr_{17}), was evaluated for hydrolysis of equine skeletal muscle myoglobin (Mb), allowing us to assess the effect of the ligand environment on protein adsorption/desorption.[34] In contrast to Hf_{18}, which only contains sulfate capping ligands, Zr_{17} provides more precise control over the ligand exchange dynamics due to its greater ligand versatility, incorporating formate, sulfate, and more labile aqua ligands.[27,35] Zr_{17} was selected over the related $Zr_{18}O_4(OH)_{38.8}(SO_4)_{12.6}(H_2O)_{33}$ (Zr_{18}) nanocluster for the same reason and also for its faster and more reliable synthesis.[36] Furthermore, by selecting a Zr- instead of Hf-based MOC, we also increase the cost-effectiveness of the cleavage protocol, since Zr(IV) is significantly less costly than Hf(IV).[37] Finally, Zr-based MOFs have consistently been reported to exhibit higher catalytic efficiency than their Hf analogs, which poses an additional incentive for developing Zr-based nanozymes.[29–30] Therefore, in this study, we performed an in-depth investigation on the factors driving protein interaction on the surface of Zr_{17} (Figure 1), highlighting the importance of the ligand exchange process at the cluster's surface. Both the cluster's charge and the reaction medium were observed to be critical in facilitating protein hydrolysis and the detection of resulting fragments. Detailed analysis of the structural stability of the core of Zr_{17} allowed for efficient catalyst recycling, which is beneficial to enhance the overall cost-effectiveness but, more importantly, essential for the cluster to compete with natural proteases for adaptation in middle-down proteomics.

Results and Discussion

Protein Hydrolysis by the Zr_{17}

Effect of Reaction Medium

The protease-like activity of the insoluble Zr_{17} was investigated in aqueous solution using the globular, heme-containing protein equine skeletal muscle myoglobin (Mb) with a molecular weight (MW) of 17.1 kDa and an isoelectric point (pI) of 6.8–7.2. Initially, the hydrolysis reactions were conducted by incubating 20 μM Mb in 1.0 mL with 2.0 μmol of solid Zr_{17} (8.7 mg) at 60 °C in water and phosphate buffer (20 mM, pH 7.4), following a similar approach (catalyst loading and reaction medium) applied in studies of previously evaluated Zr-based MOFs and the Hf_{18} cluster, allowing for comparison.[24,27,38] To monitor the reaction progress, aliquots were taken at various time intervals by separating the fine Zr_{17} powder from the reaction mixture by centrifugation and the supernatant was subsequently analyzed by sodium dodecyl sulfate-polyacrylamide gel electrophoresis (SDS-PAGE). While weak fragments at lower MW could be observed for the reaction performed in phosphate buffer (Figure S2B), no bands indicating the presence of the native protein or any generated hydrolytic fragments were observed for the reaction performed in water, which suggests complete adsorption of Mb on the cluster's surface immediately after mixing (Figure S2A). Fast protein adsorption could be identified from the color of the supernatant as well, which changed from deep red (color of Mb) to transparent.

To facilitate protein and fragment desorption, various elution protocols were applied. First, two frequently used elution buffers, glycine-HCl (3.0 M, pH 3.0) and glycine-NaOH (3.0 M, pH 9.0), were used in an attempt to disrupt protein-cluster interactions.[39,40] However, the elution process was unsuccessful as no bands originating from either the native protein or any fragments were observed after

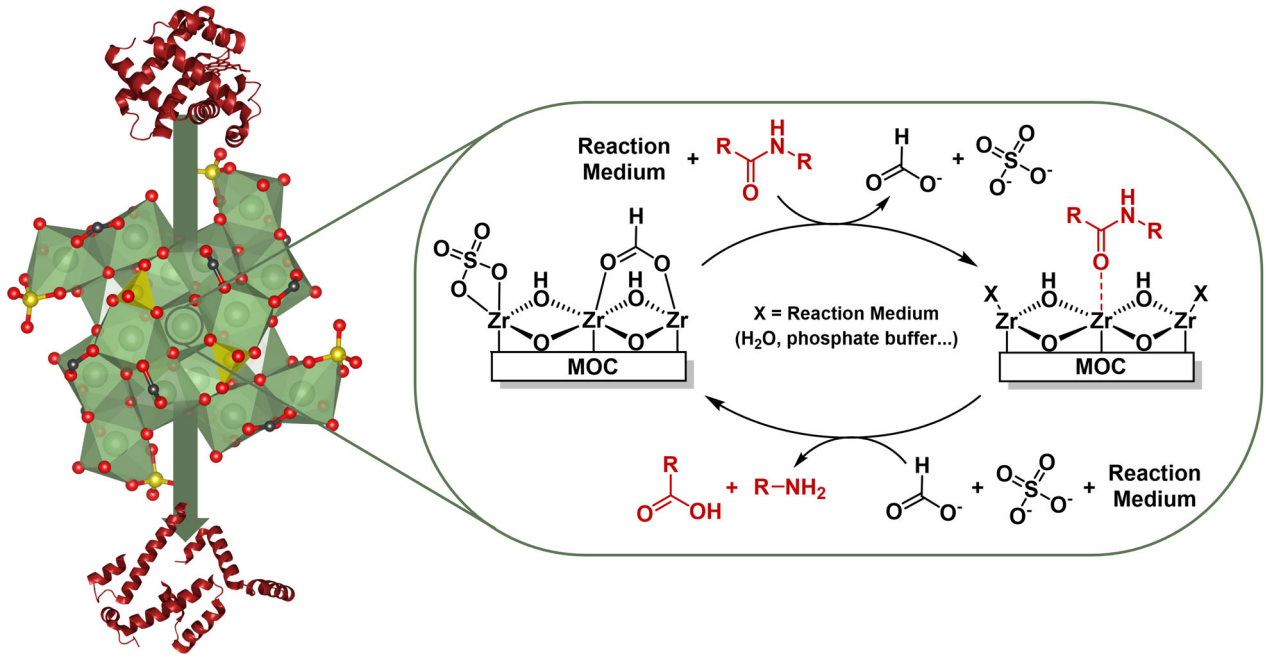

Figure 1. The ability of the $[Zr_{17}O_8(OH)_{24}(OH_2)_{12}(HCO_2)_{12}(SO_4)_8] \cdot 6\,HCl \cdot 30\,H_2O$ (Zr_{17}) solid to catalyze proteolysis is connected to the Lewis acidity of Zr(IV) in the cluster core. Substrate coordination to Zr(IV) is governed by the capping ligands and their exchange rate with the reaction medium.

incubation at 25 °C for up to 24 h (Figure S3). Therefore, the pellet after the hydrolysis reactions, containing both the cluster and adsorbed protein/fragments, was incubated in aqueous ammonia (NH_3(aq), 1%, pH 11.0) at 25 °C for up to 24 h, which was previously demonstrated to be successful in desorbing proteins from MOF surfaces.[27,29] As a result, a total of nine bands corresponding to peptide fragments with MWs of approx. 3.6, 4.8, 6.4, 7.4, 10.1, 11.7, 12.1, 13.4, and 14.7 kDa were observed after 144 h of incubation in phosphate buffer and subsequent elution (Figure S2D and S2E). However, this method was not successful for desorbing protein from Zr_{17} for reactions performed in water (Figure S2C), which prompted the development of alternative strategies.

Effect of Catalyst Loading

In order to optimize the equilibrium between protein adsorption and catalyst reactivity, thus allowing us to determine the optimal catalyst loading for the reaction, different molar amounts of Zr_{17} ranging from 0.1 to 2.0 µmol were used for hydrolysis of 20 µM Mb at 60 °C under identical reaction conditions (Figure S4). For the reactions performed in phosphate buffer, the reactivity increased linearly with the catalyst loading, where some bands were not observed in SDS-PAGE when a lower catalyst loading was applied (Figure S4B). In contrast, the reactions performed in water could not be effectively visualized by SDS-PAGE and only a limited number of fragments was detected at very low catalyst loading (0.1–0.2 µmol) (Figure S4A), which likely results from acid-induced hydrolysis since the pH of the medium decreased during the reaction (Table S1). To address the issue of protein and peptide fragment adsorption and to more accurately compare the cluster's catalytic activity in both media, the reaction mixtures consisting of different amounts of Zr_{17} and Mb incubated for 144 h were eluted using 0.2 mL 1% NH_3(aq) at 25 °C for 6 h (Figure 2a and b). The selective cleavage of Mb induced by Zr_{17} was consistent across all tested reaction conditions yielding a maximum of eight fragments. Interestingly, the adsorption of Mb and resulting fragments could be reduced by applying a lower catalyst loading, which increased the efficacy of elution. However, the number of fragments decreased at lower catalyst loading in both media, likely due to the reduced reactivity and limited adsorption capacity, ultimately leading to the complete absence of reactivity at 0.1 µmol Zr_{17}. Additionally, a lower number of fragments was observed at higher catalyst loading for the reactions conducted in water, which is most likely associated with limited protein desorption (Figure 2a). This was not observed for the reactions conducted in phosphate buffer, where greater desorption occurred (Figure 2b).

Effect of pH

Addition of Zr_{17} to water significantly acidified the medium, lowering the pH to 2.0–3.5 depending on the catalyst loading. This can be attributed to the release of the protons from the water ligands coordinated to Zr(IV) as well as the partial or complete dissolution of co-crystallized HCl within Zr_{17}. The observed decrease in pH at higher catalyst loading does not significantly affect the stability of the polypeptide chain of Mb.[22] A similar, but less pronounced decrease in pH was

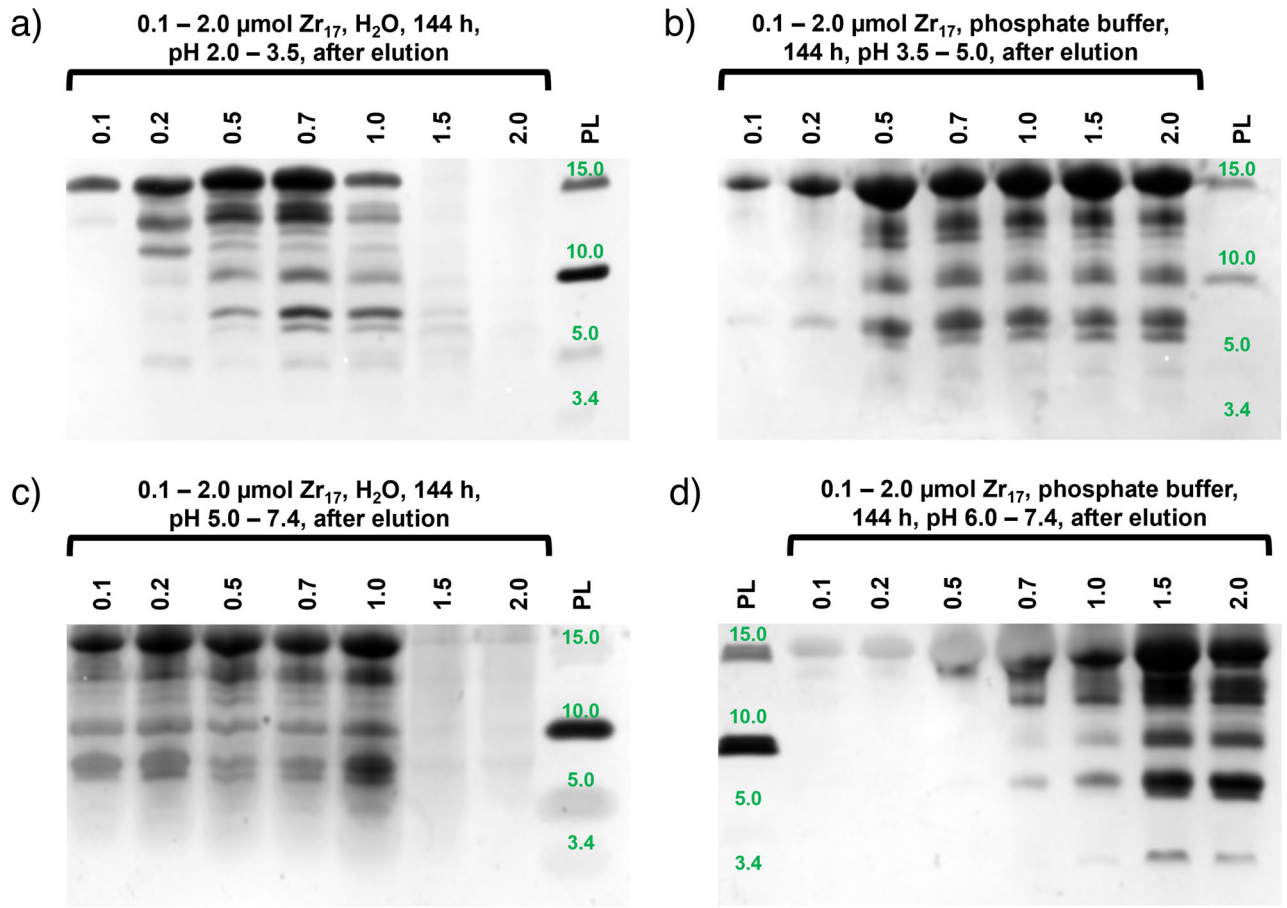

Figure 2. Silver-stained SDS-PAGE results of the eluent after hydrolysis of 20 µM Mb by 0.1–2.0 µmol Zr_{17} (144 h, 60 °C) in a) water (pH 2.0–3.5), b) phosphate buffer (pH 3.5–5.0), c) water after adjusting the pH to 7.4 (pH 5.0–7.4), and d) phosphate buffer after adjusting the pH to 7.4 (pH 6.0–7.4). The pH of the solution depends on the amount of Zr_{17} applied (Table S1).

observed for the hydrolysis reaction mixture in phosphate buffer, where the pH is in the range of 3.5–5.0 (Table S1). This indicates that the capacity of 20 mM phosphate buffer is insufficient to maintain a pH of 7.4. While an increased buffer concentration would stabilize the pH, it was previously observed that this negatively impacts the cluster's reactivity due to the formation of a protective ionic shell around the protein that prevents interactions.[27,41,42] As a result, the buffer concentration was not increased further.

In order to evaluate the influence of changes in pH on the reactivity of the Zr_{17} cluster, reaction mixtures containing 0.1–2.0 µmol Zr_{17} in 1.0 mL of 20 µM Mb in water and phosphate buffer were adjusted to pH 7.4 using 1.0 M NaOH. Addition of base stabilized the pH of the reaction mixture up to 5.0 in water and 6.0 in phosphate buffer when 2.0 µmol of Zr_{17} was applied at 60 °C for 144 h (Table S1). The produced fragments have the same MW as those generated when the pH was not adjusted, but not all fragments could be consistently visualized (Figure S5). The differences in the number of fragments most probably result from variations in the adsorption and staining process. Adjusting the pH amplifies observed trends in both water and phosphate buffer, thereby improving SDS-PAGE visualization. When the reaction was conducted in water with a high catalyst loading (1.5–2 µmol), a considerable number of peptide fragments remained adsorbed on the surface of Zr_{17}. This observation explains the reduced fragment concentration under these conditions (Figure 2c), where 24 h of elution is inadequate for the complete release of strongly adsorbed fragments. The higher reactivity of Zr_{17} in water compared to phosphate buffer is likely due to stronger retention of peptide fragments, especially at lower catalyst loading (0.1–1 µmol) where limited substrate desorption may increase turnover (Figure 2c). In contrast, weaker adsorption in phosphate buffer improves pre-elution visualization (Figure S5B) but limits the visualization of peptide fragments after elution (Figure 2d). This implies that the peptide fragments generated in phosphate buffer were largely released in solution prior to elution. Therefore, while the selectivity is identical in all tested reaction conditions, the extent of protein adsorption can be adjusted.

To confirm that acid-induced hydrolysis does not significantly contribute to cluster-induced peptide bond cleavage observed in the hydrolysis reactions where pH was not adjusted, control reactions were set up by incubating Mb in the supernatant of 2.0 µmol Zr_{17} that was previously incubated at 60 °C for 144 h in both media. The supernatant exhibits the same pH as the hydrolysis reactions conducted

with the crystalline Zr_{17} solid, likely due to release of residual HCl. No acid-induced hydrolysis was observed in phosphate buffer (Figure S6A), whereas limited hydrolysis of Mb occurred in water demonstrating a different selectivity and decreased hydrolysis efficiency in comparison to reactions in presence of Zr_{17} (Figure S6B). The supernatant controls were included in all SDS-PAGE experiments. Additional control experiments were performed by incubating Mb with HCl at a pH of approx. 2.5, resulting in limited acid-induced hydrolysis that produced a cleavage pattern distinct from that observed with Zr_{17} (Figure S6C). Finally, to ensure that the elution conditions did not cause protein hydrolysis, Mb was incubated in 1% NH_3(aq) at 25 °C for up to 24 h (Figure S6D). Complete absence of hydrolytic fragments confirms the stability of the protein under these conditions.

Comparing Hydrolysis Efficiency Across Reaction Conditions

Previous SDS-PAGE experiments indicate that both phosphate buffer and a pH of 7.0 enhance visualization of peptide fragments, particularly when applying 0.5–0.7 µmol of the catalyst. However, to ensure accurate comparison of the reactivity across all investigated reaction conditions, 0.5 µmol Zr_{17} was incubated at 60 °C in 1.0 mL of 20 µM Mb in both media, with and without adjusting the pH, and monitored for 96 h (Figure 3). Two trends can be observed: 1) the reactivity of Zr_{17} in water is similar to that in phosphate buffer with a hydrolysis efficiency of approx. 70% after 96 h in both media, and 2) hydrolysis becomes less efficient at higher pH, achieving a maximum hydrolysis efficiency of 55%–60% after 96 h for reactions at pH 7.4. However, while both the reactivity and selectivity remained identical, certain cleavage sites can be up- or downregulated depending on the reaction conditions. For example, Zr_{17} in water causes the formation of more fragments with a MW of approx. 4.8 kDa and the same reaction in phosphate buffer produces more fragments with a MW of approx. 7.4 kDa (Figure 3). However, despite these differences in the concentration of a specific polypeptide product, the protein fragments that are produced and visualized by SDS-PAGE have an identical MW. Therefore, the method allows us to tune concentrations of resulting polypeptides based on the medium and incubation time.

Selectivity of the Hydrolysis Reaction

To identify the precise cleavage sites associated with fragments observed in SDS-PAGE, HPLC-MS/MS analysis was performed. Mass spectra were collected for reactions performed in the presence of 0.5 µmol Zr_{17} in 1.0 mL of 20 µM Mb in water or phosphate buffer, incubated at 60 °C for 24 h, without adjusting pH. Supernatant control reactions were measured for both media. Elution of the cluster was not performed since MS/MS is significantly more sensitive than SDS-PAGE and not constrained by the same visualization limitations. SDS-PAGE results indicate that a maximum of nine fragments were formed with MWs of approx. 3.6, 4.8, 6.4,

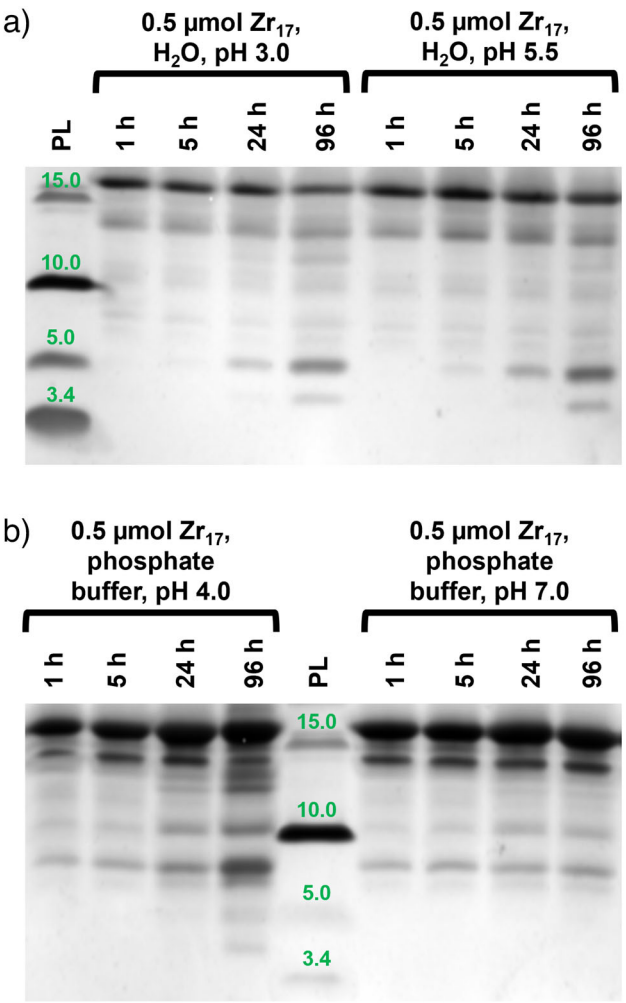

Figure 3. Silver-stained SDS-PAGE results of the eluent after hydrolysis of 20 µM Mb by 0.5 µmol Zr_{17} at 60 °C in a) water (pH 3.0–5.5) or b) phosphate buffer (20 mM, pH 4.0–7.0).

7.4, 10.1, 11.7, 12.1, 13.4, and 14.7 kDa. These peptides could result from selective cleavage at all 8 aspartate (D) residues within Mb (Table S2), however, MS/MS analysis evidenced cleavage at six out of eight D residues, namely at D5, D21, D110, D123, D127, and D142 (Figure S7 and Table S3). The D residues were cleaved at both the N- and C-terminus, consistent with the pathway proposed for Brønsted-induced D-selective cleavage.[27,43] Interestingly, cleavage at D45 and D61 sites was not observed by MS/MS analysis after 24 h of incubation (Table S3), but appearance of fragments at 6.4 and 7.4 kDa that correspond to cleavage at these sites was detected by SDS-PAGE when the incubation time was prolonged to 144 h (Figure S2).

Key Factors Influencing Protein Adsorption and Desorption

Effect of Reaction Medium and pH

In order to investigate how the reaction conditions affect reactivity and the adsorption/desorption process of the protein

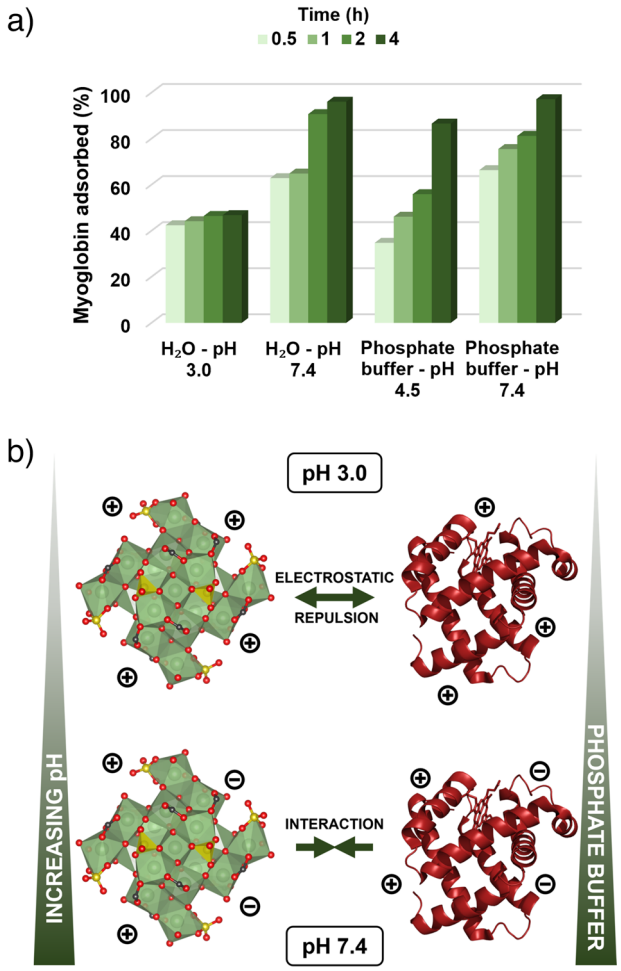

Figure 4. a) Adsorption of 20 µM Mb on 0.5 µmol Zr_{17} in water or phosphate buffer at different pH after addition of cluster in function of incubation time. b) Differences in protein adsorption are associated to the net charge of both Zr_{17} and Mb.

and peptide fragments at the surface of the crystalline Zr_{17} solid, we applied a combination of UV-Vis spectroscopy, IR spectroscopy, and isothermal titration calorimetry (ITC). The heme group present within Mb exhibits strong absorption in the visible region known as the Soret band, which arises from π-π^* transitions in the porphyrin ring. Therefore, the Mb concentration remaining in solution after incubation of 1.0 mL of 20 µM Mb with 0.5 µmol Zr_{17} could be monitored over time using UV-Vis spectroscopy (Figures 4 and S8).

Interestingly, it was observed that Mb adsorption on the surface of Zr_{17} occurred more extensively in phosphate buffer compared to water, with approx. 40% greater adsorption after 4 h, indicating stronger protein-cluster interactions. However, as shown in Figure S8A, the UV-Vis spectrum of Mb in water changes significantly after addition of Zr_{17}, with a notable shift of the Soret band from 409 to 370 nm. The changes are most probably driven by the acidic reaction conditions (pH 3.0) induced by presence of cluster. UV-Vis spectroscopy measurements of 20 µM Mb at pH 2.5–4.5 in the absence of Zr_{17} were conducted to support this statement (Figure S9), revealing a similar shift of the Soret band that indicates partial protein unfolding.[44] More pronounced adsorption of Mb on the surface of Zr_{17} was observed when the pH was adjusted to 7.4 in both media, suggesting that the net charge of the protein and cluster have a significant influence on adsorption and reactivity. Therefore, the charge of all the species in solution was analyzed by Zeta potential measurements to gain a better understanding of these results. Mb is positively charged in acidic media (approx. +30 at pH 3.0) and becomes neutral as pH increases (approx. 0 at pH 7.4) (Figure S10). Zeta potential measurements of a dispersion of insoluble Zr_{17} revealed its charge in water to be +24.10 ± 5.12 mV at pH 3.0 and -11.30 ± 4.47 mV at pH 7.4 (Figure S11) as a result of excess OH^- anions that are able to coordinate and neutralize Zr_{17}.

On the other hand, the charge of Zr_{17} in phosphate buffer was close to neutral at both pH 4.0 (+2.28 ± 8.29 mV) and 7.4 (-3.18 ± 6.23 mV) due to the presence of phosphate anions that could coordinate and neutralize Zr_{17} as well (Figure S11). Therefore, the electrostatic repulsion between the positively charged protein and cluster at low pH in water results in less effective adsorption. This electrostatic repulsion is weaker in water at pH 7.4 as well as in phosphate buffer, which enhances interaction and leads to more efficient adsorption of the protein (Figure 6 (1 → 2)).

Structural Dynamics of the Cluster's Ligand Shell

Although electrostatic repulsion at low pH explains the difference in adsorption observed by UV-Vis spectroscopy, it does not provide a rationale for peptide fragment desorption from the surface of the crystalline Zr_{17} solid observed in SDS-PAGE experiments. To address this, the structural composition of the cluster's ligand shell, consisting of coordinated formate and sulfate ligands, was evaluated by IR spectroscopy after incubation with Mb under different reaction conditions (Figure 5). The absorbance at 850–1650 cm^{-1} corresponding to the formate and sulfate capping ligands decreases after incubation of Zr_{17} with or without Mb in water, indicating their partial release from the cluster's metal centers. Interestingly, when Zr_{17} was incubated in phosphate buffer, a broad strong band at 900–1200 cm^{-1} was observed both in the presence and absence of Mb, indicating substitution of formate and sulfate with phosphate ligands that originate from the buffer solution. This exchange was confirmed by solution-state ^1H NMR analysis of the supernatant following the incubation of 2 µmol Zr_{17} in deuterated phosphate buffer at 60 °C for up to 24 h, which detected the release of approx. 63% of the formate ligands (Figure S12). To confirm that this release was specifically induced by the presence of phosphate anions, a control experiment was conducted by incubating Zr_{17} in D_2O under the same conditions, resulting in significantly reduced formic acid release (Figure S12). In addition, solid-state ^{31}P NMR analysis of Zr_{17} after incubation in phosphate buffer revealed coordination of phosphate ions, indicated by peak broadening and a downfield shift (Figure S13), resulting in 4.86 wt% bound phosphate after 24 h. Thus, it could be concluded that rapid reorganization of the cluster's capping ligands by exchange with phosphate

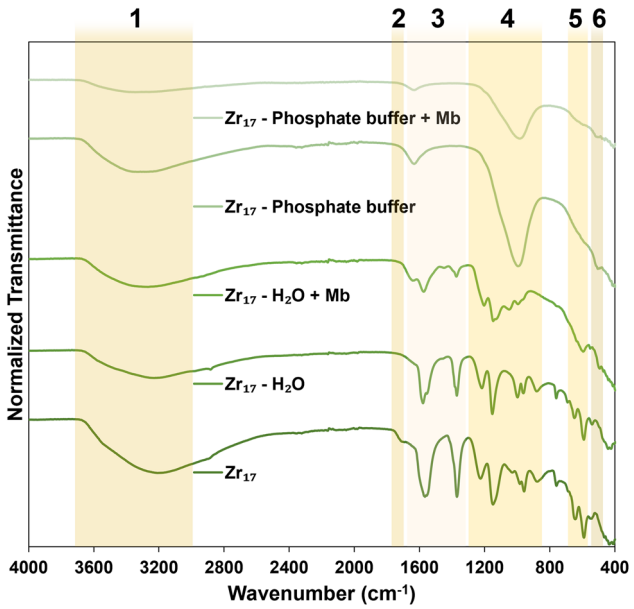

Figure 5. IR spectra of solid Zr_{17} cluster before and after incubation in water or phosphate buffer with and without Mb at 60 °C for 24 h. Absorption bands are assigned as follows: 1 and 2, OH (1700 and 3100–3700 cm^{-1}); 3, formate (COO^- at 1375 and 1571 cm^{-1}); 4 and 5, sulfate (SO_4^{2-} at 595, 652, 880, 958, 982, 1032, 1154, and 1230 cm^{-1}); 6, Zr-O(H)-Zr (543 cm^{-1}). IR spectra of Zr_{17} after incubation in pH-adjusted conditions (pH 7.4) are identical to the IR spectra at low pH.

ions, which have a strong metal-coordinating character,[45] reduces the stability of the formed peptide-cluster complexes, ultimately leading to faster desorption of generated peptide fragments in solution (Figure 6 (3 → 4)). This entails that elution is not essential for reactions performed in phosphate buffer because buffer-induced ligand dynamics play a key role in desorption (Figure S4). The enhanced adsorption and desorption processes observed in phosphate buffer compared to water may arise from various underlying processes: 1) the increased cluster charge in buffer promotes stronger initial adsorption and 2) ligand exchange with phosphate accelerates subsequent desorption. Therefore, phosphate buffer represents a desirable medium for hydrolysis catalyzed by Zr_{17}, since it is a biologically relevant medium that is able to stabilize proteins, enhance protein-cluster interaction, and simultaneously accelerate peptide desorption.

When the pH of the reaction mixture is increased to 7.4, the interaction between Zr_{17} and Mb is enhanced in both water and phosphate buffer due to more favorable electrostatic interactions, resulting in stronger adsorption (Figure 4). On the other hand, similarly to how phosphate anions enhance the exchange rate of Mb and peptide fragments with the cluster, a higher concentration of OH^- in solution also accelerates exchange, leading to more efficient desorption (Figure S5). These results suggest that the limited ligand exchange at low pH in water is responsible for the decrease in peptide fragment desorption, directly affecting fragment visualization (Figure S4). As a result, the cluster's surface remained saturated with protein and fragments, necessitating an appropriate elution protocol to efficiently release and visualize all fragments by SDS-PAGE.

To further investigate the differences in protein-cluster interaction in water and phosphate buffer, ITC was employed. The measurements were performed at 25 °C to avoid Mb hydrolysis, using dispersions of the insoluble Zr_{17} solid. This limited the range of concentrations that could be used, which, combined with the inherent complexity of the heterogeneous system, precluded quantitative data analysis and precise determination of binding constants and stoichiometries. Instead, a comparative analysis using the raw calorimetric data was performed, specifically focusing on exothermic peaks resulting from successive additions of 0.5 mM Mb to suspensions of 0.1 mM Zr_{17} (Figure S14). The heats produced by addition of Mb to Zr_{17} in water were significantly higher compared to identical measurements performed in phosphate buffer, with respective heat releases of approx. -600 and -30 µJ for the initial injections of 10 µL of Mb solution. These results can be explained by the rapid exchange of phosphate ions in solution that counterbalances the protein-cluster interaction in phosphate buffer, thereby interfering with ITC measurements and leading to lower heat release. This is in accordance with the proposed mechanism of competitive inhibition that is exacerbated by the presence of phosphate (Figure 6). However, as previously discussed, phosphate also promotes more efficient protein and fragment desorption, thereby improving visibility of fragments on SDS-PAGE and enhancing the sensitivity of the method.

Catalyst Stability

To better understand the hydrolytic results and elucidate the cluster's speciation under the tested reaction conditions, the stability of Zr_{17} was monitored by a range of techniques. IR spectroscopy of Zr_{17} before and after incubation in water or phosphate buffer and in the presence or absence of Mb indicated exchange of the ligands coordinated to the cluster core and the solvent (Figure 5). However, it does not provide any insight into the stability of the 17-nuclear cluster core. This is particularly important considering that the IR spectrum of Zr_{17} after incubation in NH_3(aq) at 25 °C for up to 24 h shows a complete absence of the absorption peaks at 850–1300 cm^{-1} and a decrease in absorption at 1300–1650 cm^{-1}, corresponding to the sulfate and formate ligands, respectively (Figure S15). This suggests that sulfate ligands, which play a key role in stabilizing the Zr_{17} cluster core, are most probably released without additional ligand substitution.

In order to assess whether the release of ligands impacts the integrity of the cluster's core and to evaluate cluster speciation after incubation, X-ray pair distribution function (PDF) analysis was employed on the solid samples. The experimental PDF of the synthesized clusters was fitted to several Zr cluster models with a nuclearity ranging from 3 to 26 (derived from known crystal structures). Among the analyzed models, the expected Zr_{17} structure resulted in the best fit with an R_W value of 0.20. All the other tested models had significantly worse R_W values of 0.35 and higher (Figures S16 and S17). A slightly improved fit is obtained using a

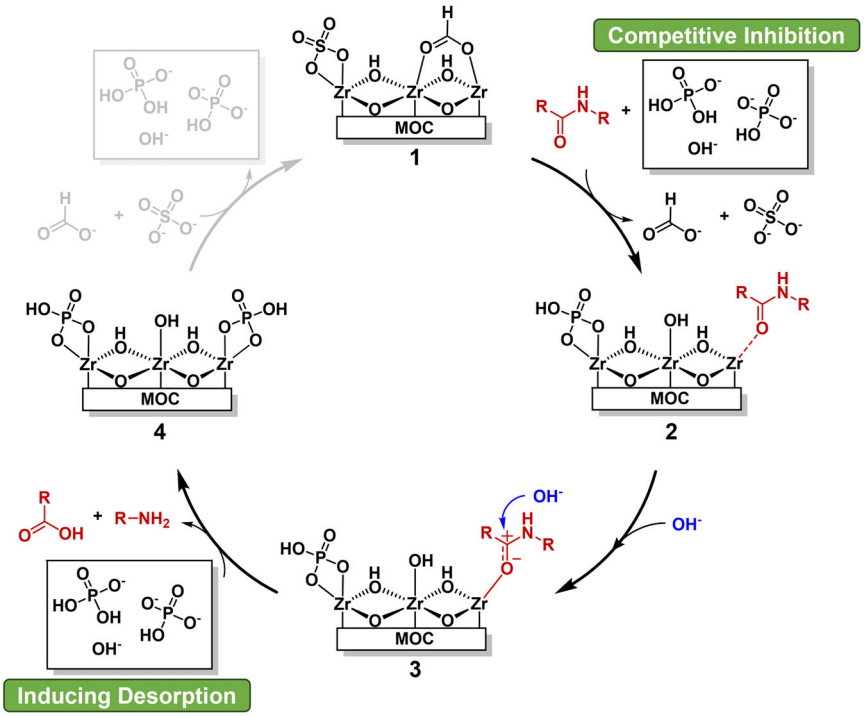

Figure 6. Proposed mechanism for Zr_{17}-catalyzed protein hydrolysis, where adsorption (1 → 2) is driven electrostatically (less repulsion at neutral pH) and desorption (3 → 4) is induced by ligand exchange (in the presence of phosphate and OH^- anions).

Zr_{17} cluster model where the atomic displacement parameters (U_{iso}) of the interior atoms (defined as within 5 Å from the geometric center) were allowed to be different from the exterior atoms (Figure 7a). The refined U_{iso} values were consistently higher for the exterior atoms compared to the interior atoms, pointing to differences in thermal motion of these atoms. This means that atoms in the exterior may have a higher flexibility while those in the interior are more rigid. The same modeling approach was used to fit all other measured samples with the Zr_{17} crystal structure.

The Zr_{17} cluster exhibited a remarkable stability across the investigated reaction conditions and environments. PDF fits revealed only minimal deviation compared to solid Zr_{17} after incubation in water and phosphate buffer at 25 °C without adjusting pH, retaining a low R_W value of 0.18 (Figure S18A). At 60 °C, the R_W slightly increased to 0.19 after incubation in water and 0.20 after incubation in phosphate buffer. These R_W values were also retained in presence of Mb at 60 °C, confirming the stability of the cluster under these conditions (Figure 7b). However, there are three exceptions where a significantly larger difference from the Zr_{17} structure was observed according to the PDF fits. Specifically, the R_W values increased to 0.24 and 0.31 after incubation of Zr_{17} in 3.0 M glycine-HCl and glycine-NaOH, respectively, and to 0.36 after incubation in 1% NH_3(aq). Figure S18B shows that peaks at higher interatomic distances were lost, indicating that the cluster either fell apart into smaller units or that it became disordered and lost its long-range coherence. This suggests that Zr_{17} exhibits reduced stability under these conditions, which most likely results from their extreme nature, that is, highly acidic and particularly alkaline media.

To ensure that soluble Zr(IV)-containing species were not produced in the investigated reaction conditions, the supernatant after incubation of cluster was analyzed using inductively coupled plasma optical emission spectroscopy (ICP-OES) (Table S5). The highest concentration of Zr(IV) was found after incubation of 2.0 µmol Zr_{17} in 1.0 mL of phosphate buffer in absence of protein for 144 h, which was 2.74 ± 0.03 ppm or 0.088 ± 0.001% of the total number of Zr(IV) atoms in 2 µmol Zr_{17}. Therefore, although very minor dissolution of Zr(IV) from the Zr_{17} cluster was observed (<3.00 ppm for all reaction conditions), its impact on protein hydrolysis is negligible compared to the impact of the insoluble catalyst.

Addition of NaOH to adjust the pH to near-neutral conditions in some reactions could lead to cluster degradation,[46] and therefore, additional experiments were conducted to confirm that the observed reactivity at higher pH (Figure 2c and d) originated from intact Zr_{17} rather than from the formation of other insoluble Zr(IV)-containing species. This concern is particularly relevant for reactions performed in phosphate buffer, where a slight decrease in activity was observed upon pH adjustment (Figure 2d). Under such conditions, the formation of zirconium phosphate species (e.g., $Zr(HPO_4)_2$ and related phases) is possible. To rule out their formation and their role in protein hydrolysis, control reactions were conducted in which 34.0 µmol $Zr(HPO_4)_2$ (the maximum theoretical amount resulting from complete degradation of 2.0 µmol Zr_{17}) was incubated with 20 µM Mb at 60 °C for up to 96 h. No fragments were detected, either directly or after elution with 1% NH_3(aq) (Figure S19), confirming that the observed hydrolytic activity in Zr_{17}-

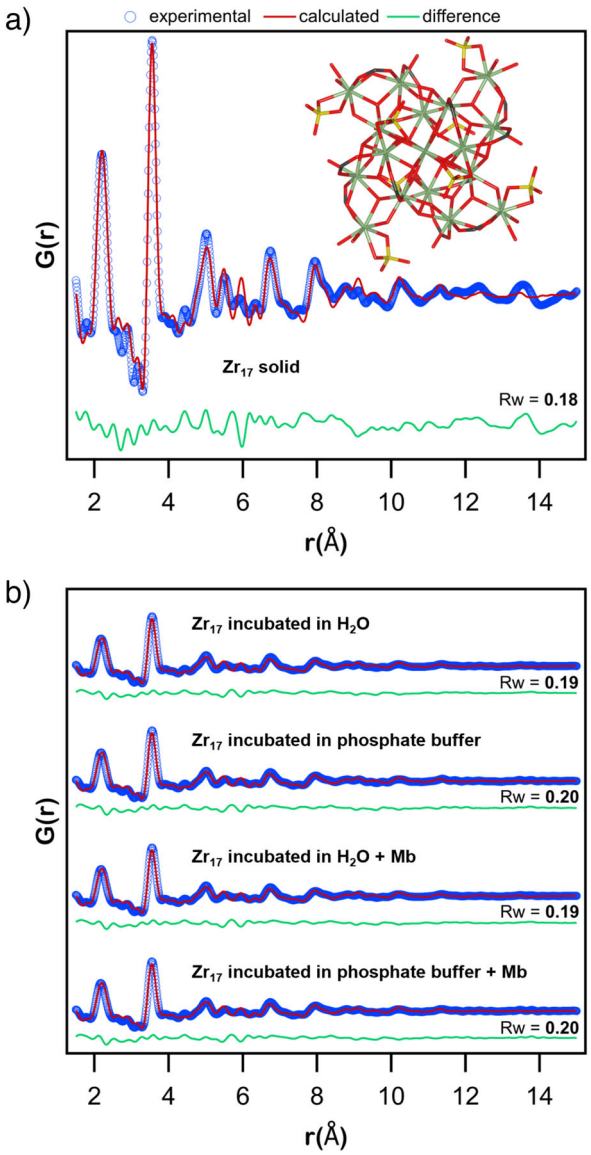

Figure 7. a) PDF fit of Zr_{17} solid with the Zr_{17} crystal structure (CCDC 1557591). b) PDF fits of Zr_{17} solid measured after incubation in water or phosphate buffer at 60 °C for 24 h in the absence and presence of Mb. The refinement parameters for all PDF fits are provided in Table S4.

containing reactions arises from the intact cluster-based solid and not from $Zr(HPO_4)_2$ that could form as a degradation product. These findings thus indicate that ligand exchange occurs without compromising the integrity of the cluster core under all tested reaction conditions.

Catalyst Recyclability

The recyclability of the crystalline Zr_{17} solid is crucial to its viability in proteomics, as it would enhance its competitiveness with established protein fragmentation methods. It has already been established that Zr_{17} remains stable under various conditions and the reaction's heterogeneous nature provides opportunity for facile separation of the Zr_{17} from the protein digest. This allows for a straightforward evaluation of the catalyst's recyclability via simple SDS-PAGE experiments. Initial attempts at recycling Zr_{17} were conducted without any elution due to the cluster's limited stability in 1% NH_3(aq). Considering that visualization of protein and fragments for reactions in water by SDS-PAGE is significantly hindered, we focused on hydrolysis reactions performed in phosphate buffer. A reaction mixture consisting of 0.5 μmol Zr_{17} in 1.0 mL of 20 μM Mb was incubated in phosphate buffer at 60 °C for 24 h. Zr_{17} was then removed and washed with phosphate buffer at 25 °C for 144 h to guarantee that any subsequent visualization of protein or formed fragments was not due to excessive adsorption on Zr_{17} (Figure S20A). Additionally, the typical Soret band of Mb could not be observed in the UV-Vis spectra of the washing solutions, which, along with SDS-PAGE results (Figure S21), indicates the complete absence of protein. The recycling process was repeated four times and after each reaction cycle, 1.0 mL of phosphate buffer containing 20 μM Mb was added to washed and dried Zr_{17} prior to incubation. The supernatant of each iteration was then analyzed by SDS-PAGE (Figure S21). The hydrolysis efficiency decreased with each cycle of the reaction, starting at approx. 60% for the first cycle and decreasing to approx. 40% by the fourth iteration. The reduced reactivity is most likely caused by the decreased acidity of Zr_{17} following the recycling process, with a pH of 4.0 during the first reaction cycle and a pH of 7.4 from the second reaction cycle onward partially due to the loss of co-crystallized HCl.

To counter the decrease in reactivity and to enable an investigation of the recyclability for reactions performed in water, an additional resynthesis step was implemented after elution in 1% NH_3(aq). The precipitate after elution was further incubated in an aqueous mixture containing 10.0 M formic acid and 0.1 M sulfuric acid at 95 °C for 24 h to regenerate the Zr_{17} structure (Figure 6(4→1)). A combination of IR spectroscopy and PDF analysis was used to verify the success of resynthesis, confirming both the ligand environment as well as the core structure of the cluster ($R_W = 0.18$) (Figures S22 and S23). A reaction mixture consisting of 0.5 μmol Zr_{17} in 1.0 mL of 20 μM Mb was incubated in water or phosphate buffer at 60 °C for 24 h and protein and fragments were eluted from the surface of the Zr_{17} using 1% NH_3(aq) at 25 °C for 6 h. After subsequent resynthesis, the process was repeated four times (Figure S20B), and each eluent was analyzed by SDS-PAGE (Figure 8). Remarkably, the hydrolysis efficiency was nearly identical in all iterations with an approximate hydrolysis efficiency of 60% after 24 h. Moreover, the pH of each reaction was similar with pH 3.0 in water and pH 4.0 in phosphate buffer. Recyclability of Zr_{17} can thus be achieved by implementing a resynthesis step. While the resynthesis process requires additional energy, formic acid, and sulfuric acid, it does not require Zr(IV), making the process more sustainable.

Conclusion

In this work, we demonstrated that the crystalline zirconium-oxo nanocluster $[Zr_{17}O_8(OH)_{24}(OH_2)_{12}(HCO_2)_{12}(SO_4)_8] \cdot 6$

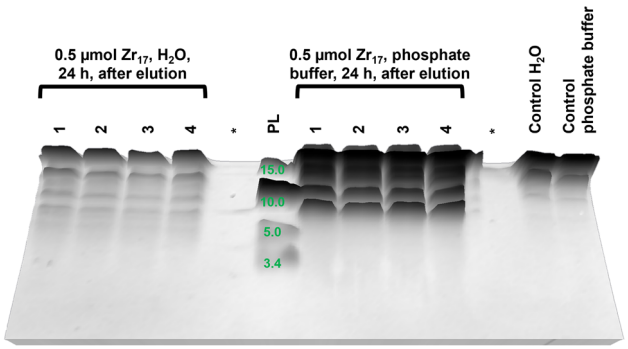

Figure 8. Silver-stained SDS-PAGE result of the eluent after hydrolysis of 20 µM Mb by 0.5 µmol Zr_{17} at 60 °C in water (pH 3.0) or phosphate buffer (20 mM, pH 4.0). 0.5 µmol of Zr_{17} was recycled for four cycles of hydrolysis reactions (1–4). The cluster was washed with water or phosphate buffer at 25 °C for 144 h after each iteration (Wash after cycle 3 is presented on the gel (*)) prior to resynthesis. A detailed explanation of the recycling process is given in Figure S19B.

$HCl \cdot 30\,H_2O$ (Zr_{17}) efficiently catalyze peptide bond cleavage across a broad range of reaction conditions. A detailed mechanistic investigation revealed that protein adsorption and subsequent protein-cluster complex formation are primarily governed by the charges of both the protein and the cluster—parameters that can be fine-tuned by adjusting the reaction environment. Regulation of the solution's pH via careful selection of the reaction medium critically impacts the stability of the formed intermediate species and facilitates rapid desorption of peptide fragments. This process is further accelerated by rapid exchange of the cluster's capping ligands, driven by the competitive coordination with buffer ions, such as phosphate. Notably, Zr_{17} consistently induced aspartate-selective cleavage across all tested conditions, while peptide product distribution could be modulated by tuning reaction parameters. The exceptional chemical stability of Zr_{17} enables its reuse over at least four protein hydrolysis cycles, significantly outperforming previously reported cluster-based catalysts. This underscores the potential of the Zr_{17} nanocluster material as a broadly applicable catalyst for site selective proteolysis. These findings offer molecular-level insight into substrate interaction with insoluble metal-oxo clusters and provide foundation for the rational design of new metal-oxo cluster-based catalysts.

Supporting Information

The authors have cited additional references within the Supporting Information.[34,47–51]

Acknowledgements

The authors thank KU Leuven (grant C14/23/088 and CELSA/24/007), Research Foundation Flanders (research grant G025624N and infrastructure grant I002720N), and the SNSF (project number 194172 and 218106) for the funding. N.D.S. (1267623N) thanks the FWO for a senior postdoctoral fellowship. They thank the Centre for Proteomics (CfP) at UAntwerp for HPLC-MS/MS measurements. They acknowledge DESY (Hamburg, Germany), a member of the Helmholtz Association HGF, for the provision of experimental facilities. Parts of this research were carried out using beamline P21.1 at PETRA III and the authors would like to thank Dr. Ann-Christin Dippel and her staff for assistance in using the beamline for PDF acquisition. Some figures were created using PyMOL.

Conflict of Interests

The authors declare no conflict of interest.

Data Availability Statement

The data that support the findings of this study are available in the Supporting Information of this article.

Keywords: Catalyst recycling · Heterogeneous catalysis · Ligand exchange · Metal-oxo cluster · Protein hydrolysis

[1] T. Klein, U. Eckhard, A. Dufour, N. Solis, C. M. Overall, *Chem. Rev.* **2018**, *118*, 1137–1168.
[2] L. Zhao, J. Zhao, K. Zhong, A. Tong, D. Jia, *Signal Transduct Target Ther.* **2022**, *7*, 113.
[3] P. Song, X. Zhang, S. Wang, W. Xu, F. Wang, R. Fu, F. Wei, *Front. Microbiol.* **2023**, *14*, 1236368.
[4] A. F. Altelaar, J. Munoz, A. J. Heck, *Nat. Rev. Genet.* **2013**, *14*, 35–48.
[5] U. A. Laskay, A. A. Lobas, K. Srzentic, M. V. Gorshkov, Y. O. Tsybin, *J. Proteome Res.* **2013**, *12*, 5558–5569.
[6] A. Aguzzi, T. O'Connor, *Nat. Rev. Drug Discov.* **2010**, *9*, 237–248.
[7] C. M. Dobson, *Nature* **2003**, *426*, 884–890.
[8] C. A. Ross, M. A. Poirier, *Nat. Med.* **2004**, *10*, S10–S17.
[9] K. P. Kepp, *Chem. Rev.* **2012**, *112*, 5193–5239.
[10] P. B. Pandeswari, V. Sabareesh, *RSC Adv.* **2018**, *9*, 313–344.
[11] L. Tsiatsiani, A. J. Heck, *FEBS J.* **2015**, *282*, 2612–2626.
[12] O. L. Tavano, *J. Mol. Catal B* **2013**, *90*, 1–11.
[13] H. Kamal, C. F. Le, A. M. Salter, A. Ali, *Compr Rev Food Sci Food Saf.* **2021**, *20*, 2455–2475.
[14] R. R. da Silva, *J. Agric. Food Chem.* **2018**, *66*, 7219–7221.
[15] C. Wu, J. C. Tran, L. Zamdborg, K. R. Durbin, M. Li, D. R. Ahlf, B. P. Early, P. M. Thomas, J. V. Sweedler, N. L. Kelleher, *Nat. Methods* **2012**, *9*, 822–824.
[16] S. R. Kundinger, I. Bishof, E. B. Dammer, D. M. Duong, N. T. Seyfried, *J. Proteome Res.* **2020**, *19*, 1574–1591.
[17] A. Cristobal, F. Marino, H. Post, H. W. van den Toorn, S. Mohammed, A. J. Heck, *Anal. Chem.* **2017**, *89*, 3318–3325.
[18] P. Giansanti, L. Tsiatsiani, T. Y. Low, A. J. Heck, *Nat. Protoc.* **2016**, *11*, 993–1006.
[19] D. E. Salazar Marcano, N. D. Savic, K. Declerck, S. A. M. Abdelhameed, T. N. Parac-Vogt, *Chem. Soc. Rev.* **2024**, *53*, 84–136.
[20] H. G. Ly, G. Absillis, R. Janssens, P. Proost, T. N. Parac-Vogt, *Angew. Chem. Int. Ed.* **2015**, *54*, 7391–7394.
[21] H. G. T. Ly, T. T. Mihaylov, P. Proost, K. Pierloot, J. N. Harvey, T. N. Parac-Vogt, *Chem. Eur. J.* **2019**, *25*, 14370–14381.

[22] K. Declerck, N. D. Savic, M. A. Moussawi, C. Seno, R. Pokratath, J. De Roo, T. N. Parac-Vogt, *J. Am. Chem. Soc.* **2024**, *146*, 11400–11410.
[23] H. G. T. Ly, G. Fu, A. Kondinski, B. Bueken, D. De Vos, T. N. Parac-Vogt, *J. Am. Chem. Soc.* **2018**, *140*, 6325–6335.
[24] S. Wang, H. G. T. Ly, M. Wahiduzzaman, C. Simms, I. Dovgaliuk, A. Tissot, G. Maurin, T. N. Parac-Vogt, C. Serre, *Nat. Commun.* **2022**, *13*, 1284.
[25] D. Conic, K. Pierloot, T. N. Parac-Vogt, J. N. Harvey, *Phys. Chem. Chem. Phys.* **2020**, *22*, 25136–25145.
[26] A. Solé-Daura, A. Rodríguez-Fortea, J. M. Poblet, D. Robinson, J. D. Hirst, J. J. Carbó, *ACS Catal.* **2020**, *10*, 13455–13467.
[27] J. Moons, F. de Azambuja, J. Mihailovic, K. Kozma, K. Smiljanic, M. Amiri, T. Cirkovic Velickovic, M. Nyman, T. N. Parac-Vogt, *Angew. Chem. Int. Ed.* **2020**, *59*, 9094–9101.
[28] H. G. T. Ly, G. X. Fu, F. de Azambuja, D. De Vos, T. N. Parac-Vogt, *ACS Appl. Nano Mater.* **2020**, *3*, 8931–8938.
[29] A. Loosen, F. de Azambuja, S. Smolders, J. Moons, C. Simms, D. De Vos, T. N. Parac-Vogt, *Chem. Sci.* **2020**, *11*, 6662–6669.
[30] J. Moons, A. Loosen, C. Simms, F. de Azambuja, T. N. Parac-Vogt, *Nanoscale* **2021**, *13*, 12298–12305.
[31] Y. Chen, V. Lykourinou, C. Vetromile, T. Hoang, L. J. Ming, R. W. Larsen, S. Ma, *J. Am. Chem. Soc.* **2012**, *134*, 13188–13191.
[32] J. G. Turner, C. J. Murphy, *Langmuir* **2021**, *37*, 9910–9919.
[33] N. Gan, Q. Sun, L. Zhao, P. Tang, Z. Suo, S. Zhang, Y. Zhang, M. Zhang, W. Wang, H. Li, *Int. J. Biol. Macromol.* **2019**, *140*, 709–718.
[34] Q. Sun, C. Liu, G. Zhang, J. Zhang, C. H. Tung, Y. Wang, *Chem. Eur. J.* **2018**, *24*, 14701–14706.
[35] Y. Xiao, B. C. Gates, D. Yang, *ACS Appl. Mater. Interfaces* **2024**, *16*, 52445–52454.
[36] P. J. Squattrito, P. R. Rudolf, A. Clearfield, *Inorg. Chem.* **1987**, *26*, 4240–4244.
[37] J. A. Sommers, L. Palys, N. P. Martin, D. B. Fast, M. Amiri, M. Nyman, *J. Am. Chem. Soc.* **2022**, *144*, 2816–2824.
[38] C. Simms, N. D. Savic, K. De Winter, T. N. Parac-Vogt, *Eur. J. Inorg. Chem.* **2022**, *2022*, e202200145.
[39] M. A. Firer, *J. Biochem. Biophys. Methods* **2001**, *49*, 433–442.
[40] P. L. Lim, *Mol. Immunol.* **1987**, *24*, 11–15.
[41] K. Stroobants, D. Saadallah, G. Bruylants, T. N. Parac-Vogt, *Phys. Chem. Chem. Phys.* **2014**, *16*, 21778–21787.
[42] G. Zhang, B. Keita, C. T. Craescu, S. Miron, P. de Oliveira, L. Nadjo, *J. Phys. Chem. B* **2007**, *111*, 11253–11259.
[43] A. Li, R. C. Sowder, L. E. Henderson, S. P. Moore, D. J. Garfinkel, R. J. Fisher, *Anal. Chem.* **2001**, *73*, 5395–5402.
[44] L. Konermann, F. I. Rosell, A. G. Mauk, D. J. Douglas, *Biochemistry* **1997**, *36*, 6448–6454.
[45] A. R. Unniram Parambil, R. Pokratath, M. J. Parammal, E. Dhaene, D. Van den Eynden, S. Balog, A. Prescimone, I. Infante, P. Shahgaldian, J. De Roo, *Chem. Sci.* **2024**, *15*, 17380–17396.
[46] I. Christodoulou, T. Bourguignon, X. Li, G. Patriarche, C. Serre, C. Marliere, R. Gref, *Nanomaterials* **2021**, *11*, 722.
[47] G. Ashiotis, A. Deschildre, Z. Nawaz, J. P. Wright, D. Karkoulis, F. E. Picca, J. Kieffer, *J. Appl. Crystallogr.* **2015**, *48*, 510–519.
[48] P. Juhás, T. Davis, C. L. Farrow, S. J. L. Billinge, *J. Appl. Crystallogr.* **2013**, *46*, 560–566.
[49] P. Juhás, C. L. Farrow, X. Yang, K. R. Knox, S. J. Billinge, *Acta Crystallogr. A* **2015**, *71*, 562–568.
[50] E. Jurrus, D. Engel, K. Star, K. Monson, J. Brandi, L. E. Felberg, D. H. Brookes, L. Wilson, J. Chen, K. Liles, M. Chun, P. Li, D. W. Gohara, T. Dolinsky, R. Konecny, D. R. Koes, J. E. Nielsen, T. Head-Gordon, W. Geng, R. Krasny, G. W. Wei, M. J. Holst, J. A. McCammon, N. A. Baker, *Protein Sci.* **2018**, *27*, 112–128.
[51] https://www.protpi.ch/Calculator/ProteinTool (accessed: 20 January 2025).

Manuscript received: June 08, 2025
Revised manuscript received: July 12, 2025
Accepted manuscript online: August 04, 2025
Version of record online: ■■, ■■